The Zirconium-Tin System, with Particular Attention to the Zr_5Sn_3-Zr_5Sn_4 Region and Zr_4Sn

Young-Uk Kwon and John D. Corbett*

Ames Laboratory[1] and Department of Chemistry, Iowa State University, Ames, Iowa 50011

Received July 31, 1989

The stoichiometric phases Zr_5Sn_3 and Zr_5Sn_4 (both $P6_3/mcm$, a = 8.4560 (7), c = 5.779 (1) Å and a = 8.7656 (7), c = 5.937 (1) Å, respectively) are obtained in high yield from powder sintering reactions of Zr and $ZrSn_2$ at 1000 °C. Arc-melted samples over the same composition range give generally complex and diffuse Guinier powder patterns, indicative of continuous distributions of compositions between the maximum melting $\sim Zr_5Sn_{3.3}$ (Zr_5Sn_3'') and either Zr_5Sn_3 or $\sim Zr_5Sn_4$. The arc-melted samples do not improve significantly on annealing at 1000–1100 °C, although the line phases are recovered if the samples are first ground and pelleted. We propose a phase diagram for this region in which the limiting phase fields Zr_5Sn_3 and Zr_5Sn_4 merge at high temperature and exhibit a common melting maximum. The overall behavior doubtlessly derives from the close structural relationship between Zr_5Sn_3 and Zr_5Sn_4, the latter (Ti_5Ga_4 type) being an interstitial tin derivative of the former (Mn_5Si_3 type). The structure of a single crystal that grew from arc-melted Zr_5Sn_3 was shown to have the intermediate composition $Zr_5Sn_{3.18}$, consistent with the proposed relationships and structures (a = 8.5036 (9), c = 5.820 (1) Å, R/R_w = 1.7/2.0%). The zirconium-richest compound in this system is a line phase with a composition between $Zr_{4.0}Sn$ and $Zr_{4.1}Sn$. The compound shows weak superstructure reflections that require a doubled cell (a = 11.252 (1) Å) and a more complex structure than the assigned A15 type. Zr_4Sn slowly decomposes to α-Zr(Sn) and Zr_5Sn_3 at 820 °C.

Introduction

The zirconium-rich region of the system zirconium–tin is important because of, among other reasons, the utility of zircaloy as fuel cladding in pressurized water reactors.[2] Nonetheless, the Zr–Sn phase diagram summary published in 1983 by Abriata et al.[3] was listed as provisional because the compositions, even the existence, of some binary phases were in doubt. The most conflicting results concerned the very questionable "Zr_5Sn_3", a compound that is particularly important relative to our subsequent studies of the extensive interstitial chemistry that is exhibited by this and structurally related compounds.[4-6] Clarification of the system in the region around Zr_5Sn_3 has therefore been the cornerstone of our reexamination of the compositions, structures, and phase relationships of binary compounds in the Zr–Sn system.

The principal source of information on the overall phase relationships for Zr–Sn is the 1953 study by McPherson and Hansen,[7] who employed mainly micrographic analysis supplemented by thermal analysis and X-ray diffraction on both as-cast and annealed samples. Westinghouse "grade 3" crystal bar zirconium was used to prepare most of the compositions of concern here, and the authors several times noted the presence of impurity phases therefrom in their products. Their study encountered unusual experimental difficulties with samples in the neighborhood of Zr_5Sn_3, in part because they found these to be exceedingly unstable toward air and/or moisture, such that freshly polished surfaces began to discolor in a matter of minutes and whole ingots disintegrated to powder in weeks. Notwithstanding, they deduced that a composition near $Zr_5Sn_{3.37}$ (40 a/o Sn) melted congruently at about 1988 °C, while as-cast samples closer to the ideal composition Zr_5Sn_3 also contained the eutectic with β-Zr. Although the former composition is close to that of Zr_3Sn_2, the compound was instead described as $Zr_5Sn_{3.4}$ with the Mn_5Si_3 structure based on unpublished work by Pietrokowsky.[8] At about the same time, Nowotny and Schachner[9] reported that a phase with a composition in the range $Zr_5Sn_{2.5}$–$Zr_5Sn_{3.0}$ and with a possibly related structure was formed in powder sintering reactions. However, this result has been subsequently discounted because of the presence of 3.3 a/o C, N, and O impurities in their zirconium and the effects that interstitial atoms are known or suspected to have on the stability of many phases with the Mn_5Si_3-type structure (Nowotny phases[10]).

A different conclusion was reached by Gran and Andersson,[11] who used X-ray powder and single-crystal diffraction to study comparable compositions after the high-purity elements had been arc-melted and then annealed at 900 °C for 2 months. They reported that the composition $Zr_5Sn_{2.5}$ gave a single phase with the Mn_5Si_3 structure, as verified by single-crystal X-ray diffraction. This they designated as Zr_5Sn_3' since the lines of a second, isostructural phase appeared in the pattern close to those of the first when the tin content was increased to that of $Zr_5Sn_{3.0}$. The latter phase had larger lattice constants and was labeled Zr_5Sn_3''. The latter plus a compound they called ZrSn (possibly Zr_5Sn_4) were both obtained at the composition $Zr_5Sn_{3.5}$. The presence of an apparent two-phase region, Zr_5Sn_3'–Zr_5Sn_3'', has contributed obvious difficulties to the description of the phase relationships,[12] and the most recent assessment[3] omitted the results of this

(1) The Ames Laboratory—DOE is operated for the U.S. Department of Energy by Iowa State University under Contract No. W-7405-Eng-82. This research was supported by the Office of Basic Energy Sciences, Materials Sciences Division.

(2) Rahn, F. *A Guide to Nuclear Power Technology*; Wiley: New York, 1984.

(3) Abriata, J. P.; Bolcich, J. C.; Arias, D. *Bull. Alloy Phase Diagrams* **1983**, *4*, 147.

(4) Corbett, J. D.; Garcia, E.; Kwon, Y.-U.; Guloy, A. *Pure Appl. Chem.*, in press.

(5) Kwon, Y.-U.; Corbett, J. D., to be submitted for publication.

(6) Garcia, E.; Corbett, J. D. *Inorg. Chem.* **1988**, *27*, 2907.

(7) McPherson, D. J.; Hansen, M. *Trans. Am. Soc. Met.* **1953**, *45*, 915.

(8) Pietrokowsky, P., Jet Propulsion Laboratory, California Institute of Technology, U.S. Army, Contract DA-04-495-ORD-18, 1952, unpublished.

(9) Nowotny, H.; Schachner, H. *Monatsh. Chem.* **1953**, *84*, 169.

(10) Nowotny, H.; Benesovsky, F. In *Phase Stability in Metals and Alloys*; Rudman, P. S., Stringer, J., Jaffee, R. I., Eds.; McGraw-Hill: New York, 1966; p 319.

(11) Gran, G.; Andersson, S. *Acta Chem. Scand.* **1960**, *14*, 956.

(12) Kubaschewski-von Goldbeck, O. In *Zirconium: Physico-Chemical Properties of Its Compounds and Alloys*; Atomic Energy Review, Special Issue No. 6, International Atomic Energy Agency: Vienna, 1976; p 121.

0897-4756/90/2802-0027$02.50/0

investigation with the speculation that the effects arose from sample inhomogeneities.

Our efforts have focused particularly on clarifying this "Zr_5Sn_3" region. The investigation has also included examination of the closely related Zr_5Sn_4 with a stuffed (Ti_5Ga_4 type) version of the Zr_5Sn_3 (Mn_5Si_3 type) structure[13] that was left out of the recent compilation because of the lack of verification and a concern about the effect of impurities.

We have also examined the composition of a phase near Zr_4Sn (Cr_3Si type, A15). Both Zr_4Sn and Zr_3Sn appear in the literature, although assignments of the latter are generally based on the ideal stoichiometry for the structure type rather than an experimental study. McPherson and Hansen[7] located this phase near 20 a/o tin by microscopy on annealed samples, although small amounts of β-Zr and Zr_5Sn_3 remained. A similar conclusion was reached by Luo et al.,[14] but no limits were placed on the composition. On the other hand, Naik and Banerjec[15] found that a Zr_4Sn stoichiometry consisted of α-zirconium and the A15 phase after annealing at 1040 °C. The face-centered tetragonal cell ascribed to this phase by McPherson and Hansen (a = 7.645, c = 12.461 Å) has not been reported since, and all other investigators have cited the cubic A15 ($Pm3n$) structure.

Experimental Section

Materials. The zirconium metal used in all experiments was reactor-grade, crystal-bar material that had principal impurities, in ppm atomic, of Fe 680, Ni 350, Hf 100 (by spark source mass spectrometry) and O 220, C 190 (by vacuum fusion). The metal was cold-rolled to sheet, cut into strips, and cleaned with a solution of concentrated HNO_3 and HF in H_2O (55:25:20 v/v). Powdered zirconium was produced through a sequence of hydrogenation, grinding, and dehydrogenation treatments of the strips. Details of the handling of the zirconium materials and of the Guinier X-ray powder diffraction methods have been given previously.[16] No impurities were evident on fusion of the tin chunks employed (Baker's analyzed, 99.99%). All powdered reactants were handled only in a glovebox. The binary phases other than Zr_5Sn_3 and Zr_5Sn_4 appear to be stable in air for weeks, and no special handling precautions were taken unless there was a particular concern about contamination before analyses by such means as single-crystal X-ray diffraction or energy dispersive X-ray (EDX) methods.

Syntheses. Arc melting, annealing, and powder sintering techniques were employed. The first was carried out under argon flow in a Centorr 5SA single-arc furnace on a water-cooled copper hearth. Zirconium was melted first as a getter. The resultant buttons were turned over and remelted at least three times in an effort to ensure homogeneity. Tin is not very volatile above the alloys, especially those in the proximity of Zr_5Sn_3, the highest melting compound in the system,[3] and only 1% excess tin was necessary to obtain the desired composition with the assumption that any weight loss arose solely from tin volatilization. Annealing treatments of the arc-melted buttons were carried out in sealed Ta tubes,[17] and these were in turn jacketed within evacuated fused silica containers for treatment in resistance-heated furnaces at 1100 °C and below. Induction heating of the Ta containers was employed at 1600 and 1700 °C (±~100 °C).

Powder sintering reactions were also utilized. Since tin is relatively soft, the compound $ZrSn_2$,[9] which can be easily ground into a powder, was employed as a reagent. Stoichiometric amounts of powdered zirconium and tin granules were loaded into a tantalum tube, this was welded, and the contents were allowed to react at 800 °C for about a week. The Guinier powder pattern calculated[18] for $ZrSn_2$ according to its reported structure type and atom coordinates[19,20] accounted for the positions and intensities of all lines very well, and the lattice parameters refined from indexed data agreed well with the literature values (see Results). Intermediate compositions were then prepared from intimate mixtures of powdered Zr and $ZrSn_2$ that were manually pressed into pellets within the glovebox with the aid of a 7-mm die set and subsequently sealed in Ta tubes for reaction.

Table I. Data Collection and Refinement Parameters for $Zr_5Sn_{3.18}$

space group	$P6_3/mcm$ (no. 193)
Z	2
lattice dimensions, Å	a = 8.5036 (9), c = 5.820 (1)
cryst dimens, mm	0.01 × 0.01 × 0.1
2θ (max), deg	60
rflctns in octants	$\pm h,k,l$
measd	1169[a]
obsd	1147
independent	248
R (av), %	1.8
R,[b] %	1.7
R_w,[b] %	2.0
second ext coeff	7.3 (5) × 10^4
abs coeff μ (Mo Kα), cm^{-1}	168.0
range of transm coeff	0.127–0.229
no. of parameters	48
no. of variables	17

[a] Systematic absences excluded. [b] $R = \sum||F_o| - |F_c||/\sum|F_o|$; $R_w = [\sum w(|F_o| - \sum|F_c|)^2/\sum w(F_o)^2]^{1/2}$, $w = 1/\sigma_F^2$.

SEM Studies. Photomicrographs and elemental analyses of some as-cast samples were obtained by using a JEOL JSM-840 scanning electron microscope and a KEVEX EDX system. Samples were dry polished with a sequence of very fine sandpapers and then ash.

X-ray Diffraction. Powder patterns were obtained on samples mounted between pieces of cellophane tape. An Enraf-Nonius Guinier camera, Cu Kα_1 radiation (λ = 1.540 56 Å), and NBS (NIST) silicon as an internal standard were employed for this purpose. The known 2θ values of the standard lines were fitted to a quadratic in their position on the film, and lattice constants of the sample then calculated by least-squares fit to indexed 2θ values.

Single-crystal X-ray diffraction analysis of a well-shaped hexagonal rod that grew from the top of an as-cast button of the nominal composition $Zr_5Sn_{3.0}$ was carried out at room temperature with the aid of a four-circle DATEX diffractometer and monochromatized Mo Kα radiation. Programs for data averaging, absorption correction, Fourier synthesis, and least-squares refinement and the source of the scattering factors have been referenced previously.[21] Some details of the diffraction data collection and refinement are listed in Table I.

The diffractometer data exhibited systematic absences of $hh\bar{0}l$ ($l \neq 2n$) reflections. The space group of the Zr_5Sn_3 (Mn_5Si_3) structure, $P6_3/mcm$, has the highest possibly symmetry meeting those conditions and was assumed on the basis of experience. A Fourier map computed after several cycles of least-squares refinement (R = 9.1%) starting with the positional parameters of Mn_5Si_3 showed a residual electron density at the origin of the unit cell (the center of the zirconium octahedra that are condensed into confacial chains). A tin atom was then included at this position, and its occupancy, along with all other variables, was ultimately refined to 0.180 (3), corresponding to the overall composition $Zr_5Sn_{3.18}$. The occupancies of all other atoms but Zr1 were also refined to confirm that all other positions in the host lattice were fully occupied to standard deviations of less than 0.7%. The largest residual in the final difference map computed

(13) Rossteutscher, W.; Schubert, K. *Z. Metallkd.* **1965**, *56*, 813.
(14) Luo, H. L.; Vielhaber, E.; Corenzwit, E. *Z. Phys.* **1970**, *230*, 443.
(15) Naik, U.; Banerjec, S. *Trans. Indian Inst. Met.* **1978**, *31*, 318. The abstract and the summary of this article are contradictory regarding the probable composition of the A15 phase.
(16) Garcia, E.; Corbett, J. D. *Inorg. Chem.* **1988**, *27*, 2353.
(17) Corbett, J. D. *Inorg. Synth.* **1983**, *22*, 15.
(18) Clark, C. M.; Smith, D. K.; Johnson, G. J. A FORTRAN IV Program for Calculating X-Ray Diffraction Patterns: Version V. Department of Geosciences, The Pennsylvania State University, University Park, PA, 1973.
(19) Laves, F.; Wallbaum, H. J. *Z. Kristallogr.* **1939**, *101*, 78.
(20) Jeitschko, W. *Acta Crystallogr.* **1977**, *B33*, 2347.
(21) Hwu, S.-J.; Corbett, J. D.; Poeppelmeier, K. R. *J. Solid State Chem.* **1985**, *57*, 43.

Table II. Positional and Thermal Parameters of Atoms in $Zr_5Sn_{3.18}$

atom	x	y	z	B_{11}[a]	B_{22}	B_{33}	B_{12}
Zr1	1/3	2/3	0	0.82 (2)	0.82 (2)	0.92 (3)	0.41 (1)
Zr2	0.252 28 (8)	0	1/4	1.67 (3)	0.84 (3)	1.73 (3)	0.42 (2)
Sn1	0.609 22 (5)	0	1/4	0.95 (2)	0.74 (2)	1.19 (2)	0.37 (1)
Sn2[b]	0	0	0	0.7 (1)	0.7 (1)	0.9 (1)	0.32 (5)

[a] The form of the anisotropic displacement parameter is $\exp[-1/4(B_{11}h^2a^{*2} + B_{22}k^2b^{*2} + B_{33}l^2c^{*2} + 2B_{12}hka^*b^*)]$. [b] Refined occupancy = 0.181 (3).

Table III. Important Bond Lengths (angstroms) in $Zr_5Sn_{3.18}$

		Intrachain			
Zr1–Zr1	2.910 (1)	Zr1–Sn1	3.001 (0)	Sn1–Sn1	4.417 (1)
Zr2–Zr2[a]	3.716 (1)	Zr2–Sn1[a]	2.918 (0)	Sn1–Sn2	3.628 (0)
Zr2–Zr2	3.615 (1)	Zr2–Sn1	3.139 (1)	Sn2–Sn2	2.910 (1)
		Zr2–Sn2[b]	2.592 (1)		
		Interchain			
	Zr1–Zr1	4.910 (1)	Zr2–Sn1[c]	3.035 (1)	
	Zr1–Zr2	3.547 (1)	Sn1–Sn1	3.452 (1)	
	Zr2–Zr2	5.120 (1)			

[a] Normal to $\vec{c}$. [b] Interstitial atom. [c] Exo bond between confacial chains.

after convergence (R = 0.017, R_w = 0.020) was ~0.2 e/Å^3 near Sn1. The refined positional and anisotropic thermal parameters and some important distances are given in Tables II and III, respectively.

Results and Discussion

The Zr_4Sn Phase (A15-Type). Samples in this region were prepared by arc-melting followed by annealing at 1000 °C for 7 days; the second step is important for a respectable yield. As before,[7] we were not able to prepare samples that were free of both β-zirconium and Zr_5Sn_3, although these were in the best cases less than about 5% each. Products of vapor-phase transport reactions (using ZrX_4) or fluxed reactions utilizing zinc gave other phases even when starting with Zr_4Sn, while sintering Zr and $ZrSn_2$ powders at 1000–1300 °C always left substantial amounts of β-Zr and Zr_5Sn_3. Annealing Zr_4Sn at 820 °C for 10 days gave significant decomposition to α-Zr and Zr_5Sn_3, as noted before.[13] This reaction may be a factor in the anomalously low-volume fractions of product observed on decomposition of α-Zr(Sn) solutions.[3,22] Study of the process is continuing.

According to our studies, the composition of this phase lies between $Zr_{4.0}Sn$ and $Zr_{4.1}Sn$ and is a line phase at 1000 °C judging from the lattice constant invariability. Whether the stoichiometry is structurally fixed at precisely 4:1 cannot be determined without a more definitive evaluation of the structure. Two obvious structural possibilities based on the A15 structure type are either vacancies ($Zr_3Sn_{0.75}$) or zirconium substitutions on the tin site ($Zr_3(Sn_{0.8}Zr_{0.2})$). A single-crystal diffraction analysis of Nb_4Ge, which has the same conflict between structure type and composition, established that it is $Nb_3(Ge_{0.8}Nb_{0.2})$,[23] and the same seems likely for Zr_4Sn. The measured density of an annealed sample with an overall Zr_4Sn composition that contained ~5% Zr_5Sn_3 was 7.10 (2) g/cm^3, closer to that calculated for the substitutional (7.22 g/cm^3) than for the (less likely) vacancy model (6.77 g/cm^3). Additional qualitative support for the substitutional model comes from a comparison of the two calculated[10] powder pattern intensity distributions with that estimated visually from the experimental pattern.

We also observe clear evidence for a superstructure, meaning that the real structure must be more complex. Doubling the exposure time for Guinier photographs reveals four more very weak but clear and reproducible reflections in addition to the 11 associated with the A15 cell (for $\theta \leq 39°$, Cu $K\alpha_1$ radiation). The pattern can be indexed with a cubic cell twice as large, viz., 11.252 (1) vs 5.6254 (7) Å for the A15 subcell.[24] A lower symmetry is thereby required. The larger cell probably arises from substitutional ordering, considering the evidently fixed composition of the phase and the character of tin solutions in α-, β-zirconium. However, our efforts to account for all of the lines and their intensities by modifying the parent structure have so far been unsuccessful. On the other hand, the reflections earlier attributed to a larger tetragonal cell[7,25] can all, with some allowance for probable uncertainties, be matched with our results plus two possible lines from α-zirconium.

$ZrSn_2$. A phase with a composition near ZrSn was estimated in the original study of this system following an electrolytic separation and chemical analysis.[7] A few years later, Hansen[26] attributed this phase to $ZrSn_2$ in the $TiSi_2$ structure based on an interim study of the latter.[9] We performed some sintering reactions around the ZrSn composition and found no evidence for an equiatomic phase.

The Zr_5Sn_3–Zr_5Sn_4 Region. Much experience has been acquired in recent years regarding A_5B_3 phases with the Mn_5Si_3 structure in which a variety of interstitial atoms may be incorporated into the center of a chain of confacial $A_{6/2}$ octahedra. Changes in the hexagonal lattice parameters are usually very sensitive, qualitative indicators of this event, including for systems like Zr_5Sb_{3+x} in which more of the main-group element can serve as a self-interstitial.[4-6,16] Therefore, the formation of a partial tin interstitial in the component with the larger cell, Zr_5Sn_3'', seemed like a reasonable postulate regarding Gran and Andersson's report[11] that two Mn_5Si_3-type phases with different sets of lattice parameters were present after arc melting and annealing. This is particularly reasonable since the subsequently discovered Zr_5Sn_4[13] (Ti_5Ga_4 type) is in fact the even larger result of the full occupancy of the interstitial site in Zr_5Sn_3 by tin. However, the reason apparently biphasic products had been obtained earlier was not clear.

Our efforts to resolve these problems and to identify the equilibrium conditions have led to the investigation of numerous reactions of the types listed in Table IV for compositions between $Zr_5Sn_{2.7}$ and Zr_5Sn_4 (33.3 and 44.4 a/o Sn). The notation of Gran and Andersson, Zr_5Sn_3' and Zr_5Sn_3'' for the smaller and larger lattice constant components, respectively, in arc-melted products is retained for the time being. The Guinier-based lattice parameters determined for all of the line phases in the Zr–Sn system

(22) Carpenter, G. J. C.; Ibrahim, E. I.; Watters, J. F. *J. Nucl. Mater.* **1981**, *102*, 280.
(23) Rasmussen, S. E.; Hazell, R. G. *Acta Crystallogr.* **1979**, *B35*, 1677.
(24) The 2θ values of the superlattice reflections for Zr_4Sn (Cu $K\alpha_1$) and their indices in the larger cell are as follows: $15.74_0°$, 200; $17.58_0°$, 210; $19.34_8°$, 211; $29.74_8°$, 321.
(25) Powder Diffraction File, JCPDS, International Centre for Diffraction Data, Swarthmore, PA, 1979; pattern no. 10-185.
(26) Hansen, M.; Anderko, K. *Constitution of Binary Alloys*, 2nd ed.; McGraw-Hill: New York, 1958; p 1219.

Table IV. Typical Results from the Reaction of Zr_5Sn_x Compositions

rctn	composition Zr_5Sn_n[a]	conditions[b]			results[c]	hexagonal phase,[d] Å	
						a	c
1	2.70	ST	1000	2 weeks	Zr_5Sn_3 + Zr_4Sn	8.4553 (7)	5.7844 (9)
2	3.00	ST	1000	2 weeks	Zr_5Sn_3	8.4547 (7)	5.7805 (9)
3	3.00	ST	1100	9 days	Zr_5Sn_3	8.4572 (7)	5.778 (1)
4	3.50	ST	1000	2 weeks	Zr_5Sn_3 + Zr_5Sn_4		
5	4.00	ST	1000	11 days	Zr_5Sn_4	8.7656 (7)	5.937 (1)
6	2.50	AM			Zr_5Sn_3' (100%, sharp pattern)	8.4752 (5)	5.7897 (7)
		AN	1150	10 days	Zr_5Sn_3' (70%) + Zr_4Sn (30%)	8.4596 (5)	5.7740 (7)
7	2.82	AM, AN	1000	1 weeks	Zr_5Sn_3' (90%) + Zr_4Sn (10%)	8.4561 (6)	5.7798 (7)
8	2.99	AM			Zr_5Sn_3' (diffuse) + Zr_5Sn_3''	8.5074 (7)[e]	5.8211 (7)[e]
		AN	1100	6 days	Zr_5Sn_3' (diffuse) + Zr_5Sn_3'' + Zr_4Sn		
9	3.08	AM, AN	1600	4 h	$Zr_5Sn_{3.1}$[f] (sharp)	8.488 (1)	5.806 (2)
10	3.26	AM			$Zr_5Sn_{3.3}$[f] (sharp pattern, "single" phase)	8.5442 (6)	5.8440 (7)
		AN	1000	15 days	$Zr_5Sn_{3.3}$ + Zr_5Sn_3' (<20%, separate and diffuse)		
11	3.4_5	AM			$Zr_5Sn_{\sim 3.4}$	8.573 (1)	5.862 (1)
		AN	1000	11 days	$Zr_5Sn_{\sim 3.4}$ + Zr_5Sn_4 (very diffuse)		
12	3.7	AM			very diffuse		
		AN	1100	11 days	Zr_5Sn_3' (~5%) + Zr_5Sn_4 (very diffuse)		
13	3.7	AM, AN	1300,	4 h	Zr_5Sn_3' + Zr_5Sn_{4-x} (both diffuse)		
14	4.0	AM			very diffuse pattern		
		AN	1700	1 h	Zr_5Sn_{4-x} (sharp) + $ZrSn_2$ (~5%)	8.7418 (7)	5.926 (1)
15	4.0	AM, AN	1000	3 days	Zr_5Sn_4 (sharp) + Zr_5Sn_3 (<5%) + $ZrSn_2$ (~5%)		

[a] ±~0.03 up to n = 3.3. [b] AM, arc-melting; AN, annealing; ST, sintering; temperatures in °C. [c] Notations for arc-melted products follow Gran and Andersson; Zr_5Sn_3'' has the larger cell, $Zr_5Sn_3' = Zr_5Sn_3$. Yields are estimated from the powder pattern intensities. [d] Space group $P6_3/mcm$. [e] Data for Zr_5Sn_3''; see text. [f] Approximate composition based on a sharp pattern for an apparently well-defined product.

Table V. Structure Types and Lattice Constants of Binary Zirconium–Tin Compounds[a]

compd	struct type	space group	lattice const, Å
Zr_4Sn	Cr_3Si (A15)	$Pm3n$	a = 5.6254 (7)
Zr_5Sn_3	Mn_5Si_3	$P6_3/mcm$	a = 8.4560 (7)
			c = 5.779 (1)
Zr_5Sn_4	Ti_5Ga_4	$P6_3/mcm$	a = 8.7656 (7)
			c = 5.937 (1)
$ZrSn_2$	$TiSi_2$	$Fddd$	a = 9.577 (1)
			b = 5.6434 (6)
			c = 9.9287 (9)

[a] Room-temperature data for equilibrium phases synthesized at 1000 °C.

are listed in Table V. The proposed phase relationships in Figure 1 build on those published for the other regions;[3] the new portions will be explained and justified in the following text.

The results in Table IV show that the nature of the products depends very much on the synthetic conditions, as already implied by various reports. Appropriate powder sintering reactions for about 2 weeks at 1000 °C produce well-defined line phases with stoichiometries Zr_5Sn_3 and Zr_5Sn_4 (to within ±0.3 a/o) and, for neighboring compositions, well-established separations into these two phases or Zr_4Sn (Table IV, reactions 1–5). Our lattice parameters for the stoichiometric phases, Table V, agree reasonably well with the earlier report for sintered Zr_5Sn_3 (a = 8.44_5, c = 5.78_5 Å, Debye–Scherrer data)[9,27] and Zr_5Sn_4 (a = 8.759, c = 5.916 Å).[13]

The arc-melting reactions with or without subsequent annealing give a variety of results. As-cast samples of compositions like $Zr_5Sn_{2.5}$ that are deficient in tin relative to Zr_5Sn_3 provide sharp powder patterns. However, these show only Zr_5Sn_3, and Zr_4Sn is seen only after annealing at 1000–1150 °C. The absence of β-zirconium from the accompanying eutectic[3] in the as-cast product is unusual. However, this fixed point is reported to be near 19.1 a/o Sn and 1592 °C and therefore to have substantially the same composition as the nominal Zr_4Sn that forms peritectoidally near 1327 °C (Figure 1). We suggest that crystal growth following substantial transformation of the intimate β-Zr–Zr_5Sn_3 eutectic mixture into Zr_4Sn during the rapid cooling of the button is insufficient for this product to be seen by X-rays. More significant in these observations is the fact that the dimensions of the Zr_5Sn_3 cell obtained from tin-poor compositions, $Zr_5Sn_{2.82}$, for example (Table IV, reaction 7, a = 8.4561 (6), c = 5.7798 (7) Å), agree well not only with those obtained for sintered $Zr_5Sn_{3.0}$ (8.4560 (7), 5.779 (1) Å average) but also with data given for Zr_5Sn_3' (8.46, 5.78 Å, respectively).[11] Therefore, Zr_5Sn_3' will hereafter be considered to be the stoichiometric Zr_5Sn_3.

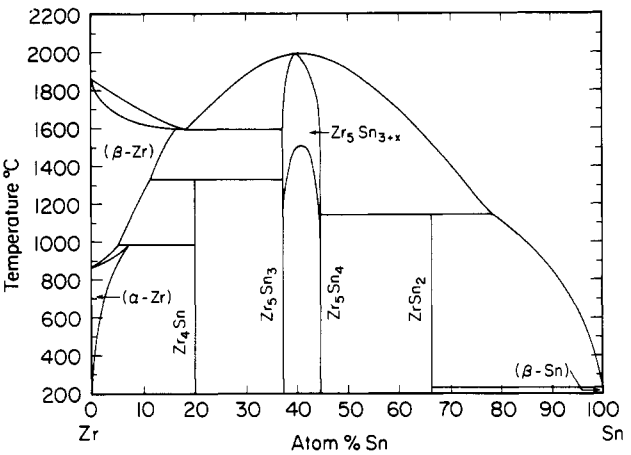

Figure 1. Proposed phase relationships between Zr_5Sn_3 and Zr_5Sn_4 added to the published, provisional diagram but with fixed point data omitted.[3] The actual solidus and liquidus boundaries in the central region have not been determined except for that of the melting maximum.

In contrast, the products of arc-melting reactions for the nominal composition Zr_5Sn_3 and beyond give more complex and frequently more diffuse powder patterns, suggesting fairly broad distributions of products. Typical line profiles for arc-melted samples across the Zr_5Sn_3–Zr_5Sn_4 region are sketched in Figure 2; the arrows mark the positions of the sharp lines for the corresponding line phases prepared by sintering. Lines in as-cast composition

(27) Nowotny, H.; Auer-Welsbach, H.; Bruss, J.; Kohl, A. *Monatsh. Chem.* **1959**, *90*, 15.

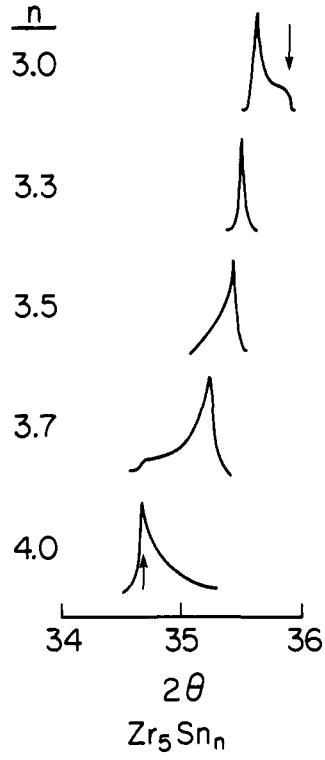

Figure 2. Line profiles of (211) reflections in Guinier patterns from arc-melted samples over the composition range Zr_5Sn_n, $3.0 \leq n \leq 4.0$. Arrows mark the positions of the (211) line in the stoichiometric end phases obtained by powder sintering.

Zr_5Sn_3 at first appearance seem to be those of a mixture of Zr_5Sn_3 with a dominant and better defined isostructural Zr_5Sn_3''. A more detailed examination shows that these actually consist of a strong and fairly sharp Zr_5Sn_3'' component paired on the high-angle side with a weak and quite uniform band that terminates in a relatively sharp edge at the Zr_5Sn_3 position. Annealing at 1000–1100 °C always gives the same mixed pattern, but Zr_4Sn is now apparent as well. Annealing an arc-melted $Zr_5Sn_{3.08}$ composition at ~1600 °C for a few hours (Table IV, reaction 9) produces a sharp, Zr_5Sn_3-like pattern with slightly greater lattice constants, but we are less confident of the composition after this more drastic treatment in a tantalum container. The lattice constants for Zr_5Sn_3'' typically fall in the neighborhood of $a = 8.5074$ (7), $c = 5.8211$ (7) Å, in close proximity to the values in the earlier report, 8.50 and 5.81 Å.[11]

In contrast to the diffuse pattern obtained for Zr_5Sn_3, that for the arc-melted $Zr_5Sn_{3.26}$ shows only very sharp lines that reflect the presence of a single, homogeneous, and well-crystallized phase (Figure 2). The expansion in the lattice constants (Table IV, reaction 10) is approximately proportional to the amount of extra tin, a further indication that these structures contain partial tin interstitials. (A similar trend has been documented for the isotypic Zr_5Sb_{3+x} system.[16]) In addition, many needlelike crystals up to 5 mm in length grow from the surface of the buttons near $Zr_5Sn_{3.26}$ during cooling in the arc furnace, to the extent that the product sometimes resembles a bundle of needles more than a button. Annealing at 1000 °C for 15 days is insufficient to attain clean phase separation from these samples, only diffuse Zr_5Sn_3 lines, not bands, being added.

Samples still richer in tin give progressively more diffuse patterns when prepared by arc melting. A $Zr_5Sn_{3.45}$ composition (Table IV, reaction 11) shows a dominant and somewhat larger cell for $Zr_5Sn_{\sim 3.4}$ plus 30–40% as much intensity distributed in a low-angle tail on each line, that is, toward the isostructural Zr_5Sn_4. The distribution broadens appreciable during the typical 1000 °C anneal. Quenched alloys of $Zr_5Sn_{3.7}$ and Zr_5Sn_4 composition provide only diffuse powder lines, corresponding to a wider range of compositions among the crystallites, and only partial separation into Zr_5Sn_3 and Zr_5Sn_4 is obtained for the former after 11 days at 1100 °C. Recognition of Zr_5Sn_4 as a new phase would be difficult under these conditions. The inhomogeneity of as-cast Zr_5Sn_4 is further demonstrated by the appearance of small amounts of both Zr_5Sn_3 and $ZrSn_2$ in the pattern after annealing at 1000 °C (Table IV, reaction 14), while a fairly sharp pattern of the substoichiometric phase plus a few lines for $ZrSn_2$ appear after a brief period at 1700 °C (±~100 °C).

A very contrasting result is achieved if these arc-melted buttons are simply ground, pressed into pellets, and sintered. The macroscopic inhomogeneities that seem evident in the arc-melted samples are clearly removed by the process, and good equilibrium phase separation is obtained. Thus, as-cast compositions Zr_5Sn_3 and $Zr_5Sn_{3.5}$ produce sharp patterns of pure Zr_5Sn_3 plus, in the latter, Zr_5Sn_4 after this procedure followed by 18 days at 1000 °C.

Phase Relationships and Distributions. The foregoing observations generally reflect the presence of sufficient compositional segregation during solidification of liquid alloys in the neighborhood of Zr_5Sn_3 and Zr_5Sn_4 that homogeneity cannot be achieved by annealing at 1000–1150 °C for up to 15 days (or 900 °C for 2 months[11]). One can construct phase relationships that are consistent with these properties. Those shown in Figure 1 build on the published, provisional Zr–Sn diagram[3] with probable relationships that can be deduced from the present study. It should be noted that none of the solidus or liquidus phase boundaries shown in the center region have been directly determined except for the congruent melting temperature and composition.

Around 1000 °C only two-line phases are present in the center region, Zr_5Sn_3 and Zr_5Sn_4, but as the temperature rises appreciably, both broaden toward each other. These must eventually join, and we have drawn one way this might occur considering the close structural relationship between the two phases (below). At even higher temperatures the phase breadth closes up toward the maximum melting point described in the original study,[7] $Zr_5Sn_{\sim 3.3}$ at 1988 °C. (The location of this is probably uncertain by up to ±0.1 in the tin coefficient or ±0.7 a/o Sn.) The phase relationships are based particularly on the distinctive powder pattern line profiles of as-cast samples (Figure 2) and the results of annealing that so clearly reflect a distribution of cell dimensions and compositions.

The phase diagram illustrates that Zr_5Sn_3, a line phase at lower temperatures, does not melt congruently and thus cannot be obtained as-cast with the usual rapid cooling, as observed. Rather, the first crystals to form have a composition in the neighborhood of $Zr_5Sn_{3.3}$, leaving the remaining liquid richer in zirconium. The lattice constants that pertain to the moderately sharp diffraction distribution seen for Zr_5Sn_3'' (Table IV) as well as to a single crystal studied (below) both suggest that the first macrocrystals have compositions near $Zr_5Sn_{3.2}$. These grow progressively poorer in tin as the button cools until they achieve the fully reduced Zr_5Sn_3 plus β-zirconium in the eutectic at ~1592 °C, in accord with the powder pattern line shapes as well as microscopy (below). Furthermore, the existence of a composition gradient within a nominal Zr_5Sn_3 sample means that equilibrium can be achieved only by diffusion over some distances. This cannot be accom-

Table VI. Intensity of Zr_5Sn_3″ Lines Relative to Those of the Adjoining Band That Ends at Zr_5Sn_3 in the Guinier Powder Patterns of As-Cast Buttons with the Overall Composition $Zr_5Sn_{3.0}$

	location in button		
	top	middle	bottom
normal melting	5	3	2
cooler arc	3		1.5
single melt	10		1.5[a]
composition near the center of the crystallites (EDX)	$Zr_5Sn_{3.24}$		$Zr_5Sn_{3.14}$

[a] Zr_5Sn_3″ is more diffuse.

plished in days to weeks at 1000 °C but can in a few hours at 1600–1700 °C where diffusion is faster, the solidus region is broad, and neighboring compositions are liquid. However, simply grinding the button to a fine powder followed by sintering of a pressed pellet at 1000 °C works equally well since most of the segregation is eliminated.

The line widths in the powder patterns of quenched alloys decrease with increasing tin content and reach a minimum, corresponding to a homogeneous (metastable) phase, near $Zr_5Sn_{3.3}$. With more tin (Table IV, reaction 11) the lines again broaden, but this time to reflect a substantial distribution of larger cells approaching Zr_5Sn_4 in size. As-cast products near $Zr_5Sn_{3.7}$ and Zr_5Sn_4 give such broad lines as to be relatively useless; annealing these near 1000 °C brings about little improvement in the former, while the pattern for the latter, though sharp, still indicates inhomogeneity by the presence of small amounts of both Zr_5Sn_3 and $ZrSn_2$. A considerable incongruity of the freezing process in the region $Zr_5Sn_{3.5}$–Zr_5Sn_4 is manifest.

An SEM-EDX study of a button of overall composition Zr_5Sn_3 that had been sectioned vertically and polished provided further details. Of additional interest are the changes seen in the diffraction intensity distribution for the Zr_5Sn_3″ component relative to the Zr_5Sn_3 band as a function of sample location within the button, the relative intensity of the arc, and whether the button has been turned over and remelted, as is customary. These are summarized in Table VI.

Electron microscopy of the top portion showed a parallel array of well-formed blades or rods ~20–50-μm wide and with very little cracking. These were separated by narrow bands of the eutectic. The crystal size and order decreased, and the amount of cracking increased downward in the button. The overall appearances were similar to those in Figures 23 and 24 in ref 7 except that our crystal sizes and the order were somewhat greater. Broad areas near the top and bottom of the button gave closely concordant compositions of $Zr_5Sn_{3.00}$ and $Zr_5Sn_{2.97}$ (±~0.01), respectively, when the overall composition was used for calibration. Thus, vertical composition gradients appear to be fairly small. In contrast, the center regions of the individual crystals near the top and bottom of the button were significantly higher in tin and somewhat different, $Zr_5Sn_{3.24}$ and $Zr_5Sn_{3.14}$, respectively. The data support the notion that growth of the original crystallites results in radial composition gradients down to Zr_5Sn_3 at their boundaries, as reflected in powder pattern line profiles.

The relative intensities of Zr_5Sn_3″ (~$Zr_5Sn_{\sim 3.2}$) lines and of the accompanying Zr_5Sn_3 band in the powder patterns of samples from different locations and melting conditions, Table VI, are also informative with regard to distributions present within samples. Either a single melt or a hotter arc serves to increase the gradients, particularly at the top of the button.

Whisker crystals often grow from the upper surface of these buttons, presumably in the last stages of solidification, and a single-crystal X-ray diffraction study was carried out on a ~10-μm-thick sample that grew from the top of a $Zr_5Sn_{3.0}$ composition (Tables I–III). The lattice constants obtained with a diffractometer, a = 8.5036 (9), c = 5.820 (1) Å, are, within the usual accuracy of this method, the same as found by Guinier methods for Zr_5Sn_3″ at the same composition, 8.5074 (7) and 5.8211 (7) Å. The overall composition refinement, $Zr_5Sn_{3.18}$, also provides a reference. Although this crystal presumably grew axially rather than radially, it may still have internal gradients and thus an average composition less than that of the melting maximum. The additional tin beyond that of the host Zr_5Sn_3 was found in the usual interstitial site within the confacial octahedral chain.

Conclusions

The more unusual results of this investigation—the inhomogeneity of many arc-melted samples, the ineffectiveness of annealing treatments, and the general nature of the apparent phase relationships in the Zr_5Sn_3–Zr_5Sn_4 region—can all be regarded as deriving from the close interconnection between the structures of Zr_5Sn_3 and Zr_5Sn_4. The unusual Mn_5Si_3-type structure of Zr_5Sn_3 (and many other compounds) affords a well-bonded arrangement with one particularly important feature: chains of zirconium octahedra that share opposite faces and are edge-bridged by tin, viz., $Zr_{6/2}Sn_{6/2}$. This feature adds a particular versatility to the chemistry of the compound in that additional atoms can often be bonded within each of these octahedra, tin in the case of Zr_5Sn_4. Although Zr_5Sn_3 and Zr_5Sn_4 are line phases at lower temperatures, it is not surprising that their close structural relationship leads to a range of nonstoichiometry (solid solution) at higher temperatures that eventually spans the region between them. The maximum melting point of this solution turns out to be about $Zr_5Sn_{3.3}$. Most of the complications arise from these last two features, as already described.

We have seen evidence of related problems in other A_5B_3–B systems where this structure type applies. Thus, Zr_5Sb_{3+x} samples can be prepared over the range $0.0 \leq x \leq 0.4$ (but not for x = 1, i.e., Zr_5Sb_4) by sintering near 1100 °C, and this solution exhibits a maximum melting point near $Zr_5Sb_{3.2}$. In this case, Zr_5Sb_3 freezes incongruently to produce $Zr_5Sb_{3.2}$ and a high-temperature polytype of Zr_5Sb_3, and their segregation again seems probable on the basis of annealing insufficiencies.[16] Not many other systems are known that contain both Mn_5Si_3- and Ti_5Ga_4-type members. However, the zirconium–gallium[28,29] and thorium–tin[30] systems would appear to be likely candidates for similar melting problems.

Finally, the interstitial chemistry of these A_5B_3 phases is by no means limited to bonding of up to one additional B element in the host. Both Zr_5Sb_3 and Zr_5Sn_3 form extensive series of Zr_5Sb_3Z and Zr_5Sn_3Z phases in the same structure with interstitial heteroatoms Z.[4-6] In the case of tin, Z includes all of the elements in the fourth period between Cu and Se as well as B to O and Al to S in the second and third periods, respectively. Most of these ternary phases, the oxide included, are stoichiometric in Z when prepared by sintering and can readily be distinguished from the binaries by their lattice constants. Some novel exceptions in stoichiometry have been found in another system, $La_5Ge_3Z_x$.[31] Nonstoichiometry, B–Z ex-

(28) Pötzschke, M.; Schubert, K. *Z. Metallkd.* **1962**, *53*, 474.
(29) Boller, H.; Parthé, E. *Monatsh. Chem.* **1963**, *94*, 25.
(30) Cirafici, S.; Palenzona, A.; Manfrinetti, P. *J. Less-Common Met.* **1983**, *90*, 49.
(31) Guloy, A.; Corbett, J. D., unpublished research.

change, and related complications are often found in these ternary systems under arc-melting conditions, as might be expected.

Acknowledgment. Slavi C. Sevov provided valuable SEM information regarding compositions of Zr_5Sn_{3+x} and Zr_4Sn as well as data on the character of the segregation present in as-case samples of the former.

Registry No. Zr, 7440-67-7; Sn, 7440-31-5; Sn_3Zr_5, 58799-99-8; Sn_4Zr_5, 12211-14-2.

Supplementary Material Available: Listing of observed and calculated structure factor data for $Zr_5Sn_{3.18}$ (1 page). Ordering information is given on any current masthead page.

Organometallic Acceptors in Molecular-Based Materials: Field-Dependent Magnetic Behavior of an Organovanadium Charge-Transfer Salt

David B. Morse

School of Chemical Sciences and the Materials Research Laboratory, University of Illinois, Urbana, Illinois 61801

Received June 6, 1989

The reaction of 2 equiv of tetramethyltetrathiofulvalene (TmTTF) with the organometallic acceptor (methylcyclopentadienyl)vanadium trichloride, $(MeCp)VCl_3$, followed by partial oxidation affords $[TmTTF]_3[\{(MeCp)VCl_2\}_2(\mu\text{-}O)]_2$ (1). The full structural parameters are reported with special emphasis on the mixed valence nature of both the cation $\{[TmTTF]_3^{2+}\}$ and anion $\{[\{(MeCp)VCl_2\}_2O]^-\}$ subunits, as well as the relationship of the two stacks within the lattice. Oriented single-crystal magnetic susceptibility data indicate that 1 develops weak ferromagnetic interactions along two dimensions (XY) at small applied fields (50 G). This behavior is dominant between 50 and 3 K. Crushed single-crystal samples require a higher applied field to induce the cooperative interactions. These cooperative interactions are suppressed at high applied fields. The zero-field ground state of 1 at 1.8 K is antiferromagnetic.

Introduction

The development of novel materials based on molecular precursors is intimately tied to the harnessing of nature's "weak forces". Secondary interactions such as those between molecules can accumulate over large distances and develop into behavior unknown at the molecular level. This kind of "supramolecule" is a species quite distinct from its molecular parents since the long-range forces allow the physical behavior of a supramolecular material to be included in an external circuit. Many current areas of interest in chemistry center about systems that rely on the accumulation of these secondary forces for their device-oriented effects. This kind of device preparation is utilized (for example) in the assembly of microelectronics,[1] molecular recognition in biosensors,[2] and the complex behavior of liquid-crystal polymers.[3]

One area in which studies of molecular-based materials has focused is the field of charge-transfer salts. These materials are composed of individually charged molecules in a solid-state lattice that governs the interactions of the subunits. Many such salts exist,[4] and the control of their secondary forces through packing arrangements is often as important as the synthesis of the individual molecules.[5] The proper combination of acceptors and donors can result in supramolecular effects such as bulk ferromagnetism[6] or superconductivity.[7]

A distinct subclass of charge-transfer salts concerns the use of high oxidation state organometallic compounds as *acceptors*. The use of organometallic *donors* in the field has shown that structurally isolated molecules can develop cooperative magnetic phenomena,[8] but the area of organometallic acceptors has only recently been investigated. The preparation of novel solid-state materials based upon organometallic complexes could prove to be a rich area, considering the synthetic diversity in organometallic chemistry. To illustrate the potential of organometallic acceptors in molecular-based materials, this paper describes the first organometallic acceptor charge-transfer salt displaying ferromagnetic coupling.[9]

Experimental Section

Synthesis. All reactions and characterizations were performed under a N_2 atmosphere using standard Schlenk line techniques and a Vacuum Atmospheres Dri-Lab. Solvents were distilled under nitrogen from appropriate drying agents (CH_2Cl_2, P_4O_{10}; toluene, Na; and hexanes, Na/K). The compound TmTTF was

(1) (a) Chao, S.; Wrighton, M. S. *J. Am. Chem. Soc.* **1987**, *109*, 2197. (b) Clarkson, M. A. *Byte* **1989**, *14*(5), 268.

(2) (a) Nagy, G.; Pungor, E. *J. Electroanal. Chem.* **1988**, *254*(20), 1. (b) Rechnitz, G. A. *Chem. Eng. News* **1988**, *66*(36), 24.

(3) Moore, J. S.; Stupp, S. I. *Macromolecules* **1988**, *21*, 1217.

(4) *Extended Linear Chain Compounds*; Miller, J. S., Ed.; Plenum: New York, 1982.

(5) Ferraro, J. R.; Williams, J. M. *Introduction to Synthetic Electrical Conductors*; Academic: Orlando, FL, 1987.

(6) Such as in $[(Me_5C_5)_2Fe][TCNE]$ (TCNE = tetracyanoethylene): (a) Miller, J. S.; Calabrese, J. C.; Epstein, A. J.; Bigelow, R. W.; Zhang, J. H.; Reiff, W. M. *J. Chem. Soc., Chem. Commun.* **1986**, 1026. (b) Miller, J. S.; Calabrese, J. C.; Rommelmann, H.; Chittipeddi, S. R.; Zhang, J. H.; Reiff, W. M.; Epstein, A. J. *J. Am. Chem. Soc.* **1987**, *109*, 769.

(7) Such as in derivatized tetrathiofulvalene complexes: Carlson, K. D.; Geiser, U.; Kini, A. M.; Wang, H. H.; Montgomery, L. K.; Kwok, W. K.; Beno, M. A.; Williams, J. M.; Cariss, C. S.; Crabtree, G. W.; Whangbo, M.-H.; Evain, M. *Inorg. Chem.* **1988**, *27*, 965, and references therein.

(8) Miller, J. S.; Epstein, A. J.; Reiff, W. M. *Chem. Rev.* **1988**, *88*, 201.

(9) Morse, D. B.; Rauchfuss, T. B.; Hendrickson, D. N. Presented in part at the 197th National Meeting of the American Chemical Society, Dallas, TX, Apr 1989; INORG 218.

0897-4756/90/2802-0033$02.50/0